Quadratic-Nonlinearity Index Based on Bicoherence and Its Application in Condition Monitoring of Drive-Train Components

Mohammed A. Hassan, *Student Member, IEEE,* Abdel E. Bayoumi, *Member, IEEE,* and Yong-June Shin, *Senior Member, IEEE*

***Abstract*—A new concept of Quadratic-Nonlinearity Power-Index spectrum, $QNLPI(f)$, that can be used in signal detection and classification, is proposed based on bicoherence spectrum. The proposed $QNLPI(f)$ is derived as a projection of the three-dimensional bicoherence spectrum into two-dimensional spectrum that quantitatively describes how much of the mean square power at certain frequency f is generated by nonlinear quadratic interaction between different frequencies. The proposed index, $QNLPI(f)$, can be used to simplify the study of bispectrum and bicoherence signal spectra. It also inherits useful characteristics from the bicoherence such as high immunity to additive gaussian noise, high capability of nonlinear-systems identifications, and amplification invariance. Concept of the proposed index and its computational considerations are discussed first using computer generated data and then applied to real-world vibration data from a helicopter drive-train to assess health conditions of different mechanical faults as part of condition based maintenance (CBM).**

***Index Terms*—Higher-Order Statistics (HOS), Bispectrum, Bicoherence, Condition-Based Maintenance (CBM), Helicopter Maintenance, Vibration Monitoring.**

I. INTRODUCTION

CONDITION based maintenance (CBM) is an approach where troubleshooting and repairing machines are performed based on continuous monitoring of their part's conditions [1]-[5]. Nevertheless, maintenance actions are taken based on observation and analysis rather than following a strict maintenance time schedule as in the case of time based maintenance (TBM). Over the past decade, success in achieving CBM goals has resulted in large-scale deployment of HUMS (Health and Usage Monitoring Systems) in military helicopters using Vibration Management Enhancement Program (VMEP) hardware [6], [7]. Condition monitoring of critical components in the aircraft is achieved through processing variety of time-varying signals (waveforms) collected using sensors attached to those critical components. The vibration signals are the most common and popular waveform data used in condition monitoring of rotating and reciprocating components [8]-[13].

Bispectrum and its normalized version bicoherence have shown to be useful tools in machine condition monitoring fields (e.g., [14]-[20]). One of the major advantages of using bispectrum over the conventional power spectral density is its ability to detect and to quantify quadratic nonlinearities associated with machine faults. The nonlinearities result in various frequencies to mix forming new spectral components in frequency domain that exhibit phase coherence to the primary interacting frequencies. Bispectrum describes this frequency coupling relation between the source and the result of the interaction process in bi-frequency space.

However, investigation of quadratic nonlinearities using bispectrum/bicoherence becomes a challenging task when the studied signal contains wide range of frequency interactions. The three dimensional nature of these spectra requires careful design of the view and expert personnel to interpret the results in the frequency domain. Therefore, it is easier to use features extracted from those spectra to summarize and describe nonlinearities in the monitored signals. For example; bispectrum mean-magnitude and phase-entropy have been used in blind detection of photo-montage [21], normalized bispectrum entropy and normalized bispectrum squared entropy have been used in health assessment of human cardiac [22], and invariant phases of integrated bispectrum has been used to detect mines in acoustic images [23], [24]. Since machine fault diagnostic is better archived by linking certain frequency to a particular rotating component, quadratic-nonlinearity power-index ($QNLPI(f)$) spectrum has been proposed as a way to summarize information in the 3D bicoherence into 2D frequency spectrum [25].

In this paper, the proposed concept of the $QNLPI(f)$ is discussed in more details including considerations in its computation and boundary limits. The quadratic-nonlinear power spectral density $P_{QNL}(f)$ and percentage of quadratic nonlinear power $PQNLP$ are also introduced based on the $QNLPI(f)$, as will be discussed in section II. Based on higher order statistical (HOS) analysis, this paper presents applications of the proposed nonlinearity measures to real-world vibration data obtained from a dedicated condition based maintenance experimental helicopter drive-train, as will be shown in section III. Health condition of different rotating components in the drive train is assessed including different combinations of drive-shaft and gearbox faults. The $QNLPI(f)$ spectrum enables us to gain more details about nonlinear harmonic generation patterns that can be used to distinguish between different cases of mechanical faults, which in turn helps to gaining more diagnostic/prognostic capabilities.

Mohammed A. Hassan is with the Department of Electrical Engineering at the University of South Carolina, Columbia, SC, 29208 USA.

Abdel E. Bayoumi is with the Department of Mechanical Engineering at the University of South Carolina, Columbia, SC, 29208 USA.

Yong-June Shin is with the Department of Electrical and Electronic Engineering at Yonsei University, Seoul 120-749, Korea. Corresponding author: (yongjune@yonsei.ac.kr).

Part of this paper was presented at I2MTC 2012.

II. Quadratic-Nonlinearity Power-Index Spectrum

Higher order spectra (polyspectra) are spectral representation of higher order moment or cumulant statistics. The bispectrum $B_x(f_1, f_2)$ for a zero-mean stationary random signal $x(t)$ is the third order spectrum and it is defined as follows [26]:

$$B_x(f_1, f_2) = E\{X(f_1)X(f_2)X^*(f_1 + f_2)\} \tag{1}$$

where $E\{.\}$ denotes an expected value operator, $X(f)$ is the Fourier transform of $x(t)$, and * denotes a complex conjugate. For a given experimental situation, we generally do not have knowledge of the relevant joint probability density function. Therefore, in practice, the expected value operation in equation (1) is carried out using average over ensemble of a collected sample spectra.

Symmetry properties of the bispectrum in addition to Nyquist frequency limit imply that when bispectrum is digitally computed, it is usually plotted over the triangle area denoted "A" that is bounded between the three lines $f_2 = 0$, $f_2 = f_1$, and $f_1 + f_2 = f_S/2$ in the $f_1 - f_2$ plane, shown in Figure 1, where f_S is the sampling frequency [26].

The definition of the bispectrum in (1) shows how it measures phase coupling in three signals due to quadratic nonlinearity where $B_x(f_1, f_2)$ will be zero unless the following two conditions are met:
(a). Signals must be present at the frequencies f_1, f_2, and $f_1 + f_2$. That is, $X(f_1)$, $X(f_2)$, and $X(f_1 + f_2)$ must be non-zero, and
(b). A phase coherence must be present between the three frequencies f_1, f_2, and $f_1 + f_2$.

Thus, the magnitude of the bispectrum at coordinate point (f_1, f_2) measures the degree of phase coherence between the three frequency components f_1, f_2, and $f_1 + f_2$. However, this magnitude is also dependent on the magnitude of the relevant Fourier coefficients. Therefore, a common function used to normalize the bispectrum magnitude is the bicoherence $b_x(f_1, f_2)$ [27] as given in equation (2).

$$b_x^2(f_1, f_2) = \frac{|B_x(f_1, f_2)|^2}{E\{|X(f_1)X(f_2)|^2\}E\{|X(f_1 + f_2)|^2\}} \tag{2}$$

The bicoherence in (2) is independent of the magnitude of the Fourier transform and bounded by $0 \leq b_x(f_1, f_2) \leq 1$, where unity means full three-waves coupling (i.e., interaction has taken place between the waves), and zero implies an absence of coherence or interaction. Moreover, it has been proven in [27] that the squared bicoherence, $b_x^2(f_1, f_2)$, quantifies the fraction of mean square power at $f_3 = f_1 + f_2$ due to the quadratic coupling between the waves at f_1 and f_2. This previous property inspired us to propose a metric that shows the quadratic interaction relation (3 waves coupling) in terms of the "result" instead of the "source" of the interaction. Hence, the bi-frequency space required to plot the bicoherence (showing the source of interaction) can be reduced to a single-frequency space (showing the accumulative results).

The Quadratic-Nonlinearity Power-Index, $QNLPI(f)$,

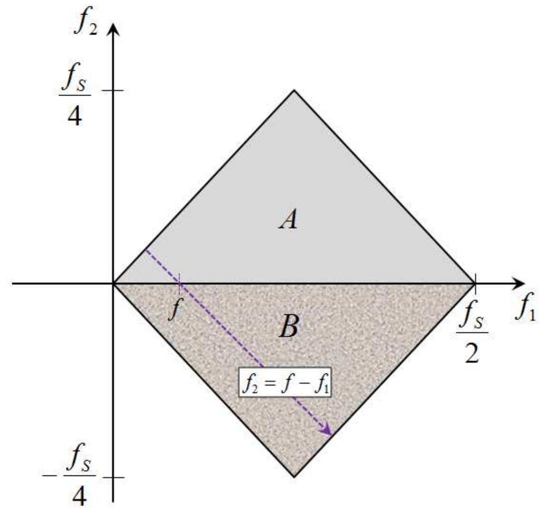

Fig. 1. Region of computation (ROC) for the bispectrum/bicoherence assuming aliasing is absent: triangle "A" is the conventional ROC, region "$A - B$" is used to calculate the proposed $QNLPI(f)$, and dashed line indicates the direction of integration to calculate the $QNLPI(f)$

spectrum is proposed as an implementation of the idea discussed above, and hence it should quantify the fraction of the mean square power at a certain frequency f produced by all the possible combinations of quadratic interactions that may cause the creation of this frequency, f. This idea can be achieved by integrating the bicoherence spectrum along a straight line $f_1 + f_2 = f$ represents the locus of all quadratic interactions in $f_1 - f_2$ space that result in f, as represented by equation (3).

$$QNLPI(f) = \int_{f_1+f_2=f} b_x^2(f_1, f_2)\, df_1 \tag{3}$$

This integration along $f_1+f_2 = f$ is depicted by the dashed line in Figure 1. However, we should be very careful when we apply this integration in (3) to the conventional region of computation indicated by the triangle "A" shown in Figure 1. Due to the symmetry properties, the bicoherence of interacted frequencies in the fourth quadrant (positive f_1 and negative f_2) has a redundant copy in this "A" region. Therefore, the region of computation in $f_1 - f_2$ plane is modified to fully map the quadratic interaction between different frequencies as shown in Figure 1. The area covered by triangle "B" maps the difference part of the interaction between two frequencies $(f_1, -f_2)$, while area covered by the upper triangle "A" maps only the sum part (f_1, f_2). Based on this new region of computation, $QNLPI(f)$ in (3) can be rewritten as follows:

$$\begin{aligned} QNLPI(f) &= \int_{\frac{f}{2}}^{\frac{f}{2}+\frac{f_S}{4}} b_x^2(f_1, f - f_1)\, df_1 \\ &= \int_{0}^{\frac{f_S}{4}} b_x^2(\frac{f}{2} + f_1, \frac{f}{2} - f_1)\, df_1 \end{aligned} \tag{4}$$

Equation (4) indicates that all the information contained in the bicoherence is represented in the $QNLPI(f)$ which is function in one variable, f. Moreover, the $QNLPI(f)$ inherits useful characteristics from the third order statistics, bicoherence, such as high capability of nonlinear-systems identifications, high immunity to additive gaussian noise, and amplification invariance. Furthermore, it can be proven that $QNLPI(f)$ is theoretically bounded between zero and one ($0 \leq QNLPI(f) \leq 1$) as shown in appendix A. Zero value of $QNLPI(f)$ means that no quadratic-nonlinearity produces any power at this frequency, while one means all the power at frequency f result from quadratic-nonlinearity.

A. Digital Computation of QNLPI(f)

The same procedure described in [27] can be followed in order to calculate digital bicoherence taking into consideration the modified region of computations described before in Figure 1 to separate and account for both positive and negative parts of frequency interactions. Next, digital computation of the $QNLPI(f)$ can be carried out by replacing integration in (4) by summation as shown in (5).

$$QNLPI(f) = \sum_{n=0}^{n=\frac{N}{2}-1} b_x^2((\frac{f}{2}+n\Delta f),(\frac{f}{2}-n\Delta f)) \quad (5)$$

where Δf is the elementary band width determined from the resolution of DFT calculation. $\Delta f = f_N/N$, $f_N = f_S/2$, and N is the number of points used in DFT calculation. The frequency resolution Δf should be smaller than the difference between the smallest two frequencies expected to interact in any particular case.

B. Nonlinear Power Spectral Density

Power spectral density $P_x(f)$ is the Fourier transform of the auto-correlation function $R_x(\tau)$ for a stationary random process $x(t)$ according to Wiener-Khintchine theorem [28]. Thus, it can be estimated using the following equation:

$$P_x(f) = E\{X(f)X^*(f)\} = E\{|X(f)|^2\} \quad (6)$$

$P_x(f)$ has the dimensions of mean square values/Hz and it indicates how the mean square value is distributed over frequency.

Based on the proposed $QNLPI(f)$ index discussed in the preceding subsection, one can estimate how much of the mean square power at certain frequency is generated due to the second order nonlinearity by multiplying the $QNLPI(f)$ index at this frequency by the power spectral density $P_x(f)$, as follows:

$$P_{QNL}(f) = QNLPI(f) \cdot P_x(f) \quad (7)$$

where $P_{QNL}(f)$ is the nonlinear power spectral density showing the distribution of quadratic-nonlinearly-generated mean square power over frequency, and it also has the dimensions of mean square values/Hz. Thus, integration of $P_{QNL}(f)$ over the whole range of frequencies estimates the total quadratic nonlinear power contained in the signal. It would be also useful to quantify the percentage of quadratic nonlinear power ($PQNLP$) to the total mean square power as follow:

$$PQNLP = \frac{\sum_{n=0}^{N-1} QNLPI(n\Delta f) \cdot P_x(n\Delta f)}{\sum_{n=0}^{N-1} P_x(n\Delta f)} \quad (8)$$

where denominator in equation (8) estimates the total power in the signal while the numerator estimates the overall quadratic nonlinear power. $PQNLP$ is a single-value metric that is useful in monitoring the severity of nonlinear behavior of the signal under study which can be used to monitor fault-progress, as will be shown in section III-C.

C. Numerical Example of QNLPI(f)

Before we apply the proposed indices to study nonlinear coupling in real world vibration data, we will use simple signal to illustrate the usefulness of these metrics and help understand the physical interpretation of their values. Thus, a computer-generated test signal has been used as shown in equation (9).

$$\begin{aligned} x(t) = {} & A_b\cos(2\pi f_b t+\theta_b) + A_c\cos(2\pi f_c t+\theta_c) \\ & + A_e\cos(2\pi f_e t+\theta_e) + A_g\cos(2\pi f_g t+\theta_g) \\ & + A_{bc}\cos(2\pi f_b t+\theta_b)\times\cos(2\pi f_c t+\theta_c) \\ & + A_{eg}\cos(2\pi f_e t+\theta_e)\times\cos(2\pi f_g t+\theta_g) \\ & + A_d\cos(2\pi f_d t+\theta_d) + n(t) \end{aligned} \quad (9)$$

$A_b = A_c = A_d = A_e = A_g = 2, A_{bc} = A_{eg} = 4$, sampling frequency $f_s = 2f_N = 4.8$ kHz, $f_b/f_N = 0.22, f_c/f_N = 0.375, f_e/f_N = 0.292, f_g/f_N = 0.303$ and $f_d = f_b + f_c = f_e + f_g$. All the phases are independently taken from a set of uniformly distributed random numbers. The $n(t)$ is a small amplitude additive Gaussian noise (-20dB) to simulate the maximum estimated noise levels in our experimental setup.

In this testing signal $x(t)$, the total power at f_d is a share of three equal source; the independent excitation, the quadratic nonlinear interaction between f_b and f_c, and the quadratic nonlinear interaction between f_e and f_g. The power spectrum of the test signal, the modified bicoherence $b_x^2(f_1, f_2)$, the quadratic-nonlinearity power-index $QNLPI(f)$, and the quadratic-nonlinear power spectrum $P_{QNL}(f)$ are shown in Figure 2.

From Figure 2-(b), $b_x^2(f_c, f_b) = 0.324$, and $b_x^2(f_g, f_e) = 0.329$ are lined up on the same $f_1 + f_2 = f_d$ axis. This means that each group contributes to the quadratic-nonlinearity power-index in Figure 2-(c) by approximately one third. $b_x^2(f_g, -f_e) = 1$ and $b_x^2(f_c, -f_b) = 1$ lie in the "B" zone of the modified bicoherence and represent the negative part of the interaction for both $f_c - f_b$ and $f_g - f_e$. The detailed bicoherence spectrum in Figure 2-(b) is represented by the $QNLPI(f)$ in Figure 2-(c). $QNLPI(f_d) = 0.653$ which means that two-thirds of the total power at frequency f_d is coming from quadratic-nonlinear interaction between different frequencies. Putting the $QNLPI(f)$ along with the power spectrum of the signal would help to better understand some

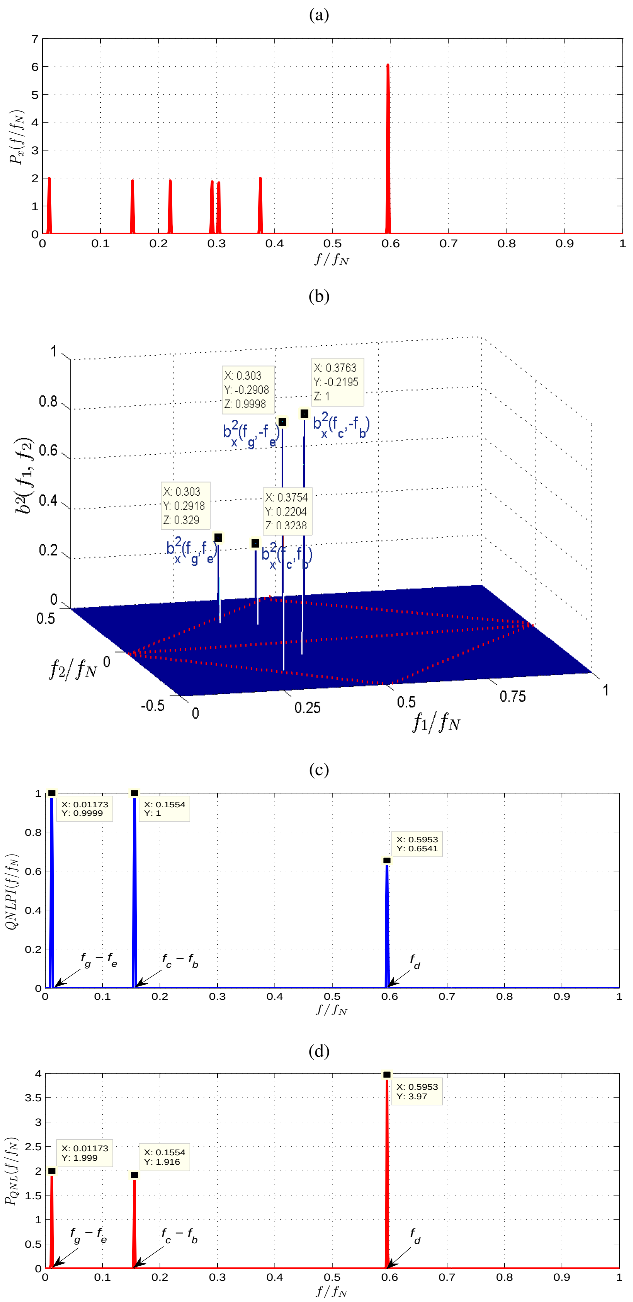

Fig. 2. (a) Power spectral density, (b) Modified bicoherence, (c) QNLPI, and (d) Quadratic-nonlinear power spectral density; for test signal in (9)

details about the signal that is not clear in the power spectrum alone. The power spectral contents that generated only by quadratic nonlinearity are separated in the $P_{QNL}(f)$ as shown in Figure 2-(d). Total quadratic-nonlinearity in this signal is quantified using the percentage of quadratic nonlinear power ($PQNLP$) presented in equation (8) and the $PQNLP$ is found to be = 42.93%.

III. Application of $QNLPI(f)$ in Health Assessment of Helicopter Drive Train Components

We now demonstrate the application of the proposed $QNLPI(f)$ by using two different real-world vibration data to assess health conditions of rotating mechanical components in an Apache helicopter tail-rotor drive-train. In the first case, nonlinearity signature of different fault types associated with drive shafts are studied in subsection III-B. In the second case, development of nonlinearity in the vibration collected from faulted gearbox is studied as will be discussed in subsection III-C.

A. AH-64 tail rotor drive train test stand

The CBM center at the University of South Carolina (USC) has a complete AH-64 (Apache helicopter) tail rotor drive train (TRDT) test stand for on-site data collection and analysis, as shown in Figure 3-(b). The TRDT test stand emulates the complete tail rotor drive train from the main transmission tail rotor takeoff to the tail rotor swash plate assembly, as shown in Figure 3-(a).

All drive train parts on the test stand are actual aircraft hardware. The prime mover for the drive train is an 800hp AC induction motor controlled by variable frequency drive. An absorption motor of matching rating is used to simulate the torque loads that would be applied by the tail rotor blade and it is controlled by another variable frequency drive. The signals being collected during the operational run of the apparatus include vibration data measured by the accelerometers, temperature measured via thermocouples, and speed and torque measurements. The measurement devices are placed at the forward (FHB) and afterward (AHB) hanger bearings and two gearboxes as shown in Figure 3-(b).

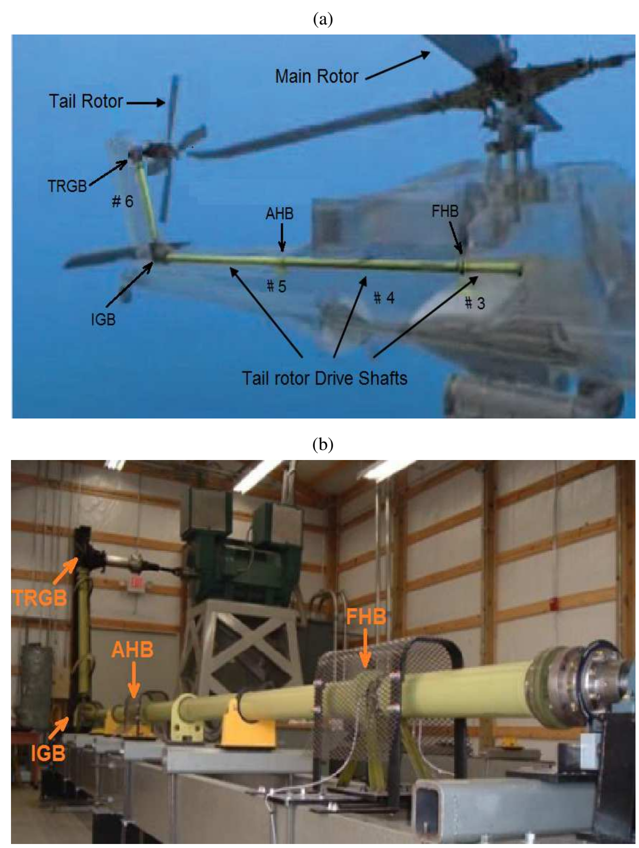

Fig. 3. (a) Actual TRDT on AH-64, and (b) TRDT test stand at USC

B. $QNLPI(f)$ of different drive-shaft faults

Focus of this study is centered on studying different combinations of drive-shafts faults using both conventional power spectral density (PSD) and the proposed $QNLPI(f)$. Shafts numbered 3-5 in Figure 3-(a) operate at a rotation speed of 4863 RPM (81.05Hz) corresponding to full-speed of shaft rotation on the fielded rotorcraft. The vibration signals denoted as FHB and AHB, measured at forward and afterward hanger bearings respectively, are gathered at two minutes intervals at a sampling rate of 48 kHz over the course of thirty minute test runs. The measurements are taken for different drive-shafts setting under test which include baseline shaft and bearing configuration, unbalance in different shafts configuration, and shaft misalignment, all common issues on AH-64 drivetrains. Misalignment of the shafts is studied at 1.3° between drive-shafts #3 and #4, 1.3° between drive-shafts #4 and #5. Unbalance is studied at drive-shafts #3, #4 and #5 by 0.140 oz-in, 0.135 oz-in 0.190 oz-in respectively. Different combination of misalignment and unbalance are tested with Table I summarizing these test conditions and their coded designations.

TABLE I
TAIL ROTOR DRIVESHAFT EXPERIMENTAL SETTINGS

Shaft Status	Balanced	Unbalanced
Aligned	00321	10321
Misaligned	20321	30321

Due to the loading scheme of the TRDT test stand with the intermediate gear box (IGB) and the output motor torque, the 3^{rd} harmonic of the tail rotor drive shaft (243 Hz) is dominating the power spectrum of the AHB vibrations in the studied cases with some other different harmonics in each setting, as shown in Figures 4 and 5. The power spectra of the baseline (00321) and the misaligned (20321) cases in Figure 4 have the same dominating spectral peaks with very slight changes in the minor peaks. A similar situation occurs when we compare the unbalanced (10321) and the misaligned-unbalanced (30321) cases in Figure 5. It is not an easy task to distinguish between different cases by looking at the whole power spectrum.

Conventional PSD comparison with the baseline is usually done on a logarithmic amplitude scale with increases of 6-8 dB considered to be significant and changes greater than 20 dB from the baseline considered serious [29]. Table II summarizes the results of the spectral peak comparison of the three faulted cases (10321, 20321, and 30321) with the baseline case (00321) in terms of the first three spectral

TABLE II
COMPARISON WITH BASELINE CASE IN TERMS OF SP1, SP2, AND SP3 (DB)

	A/UB(10321)	MA/B (20321)	UB/MA(30321)
SP1	5.311	-0.081	4.799
SP2	9.997	10.255	8.661
SP3	-2.001	-2.0667	-8.141

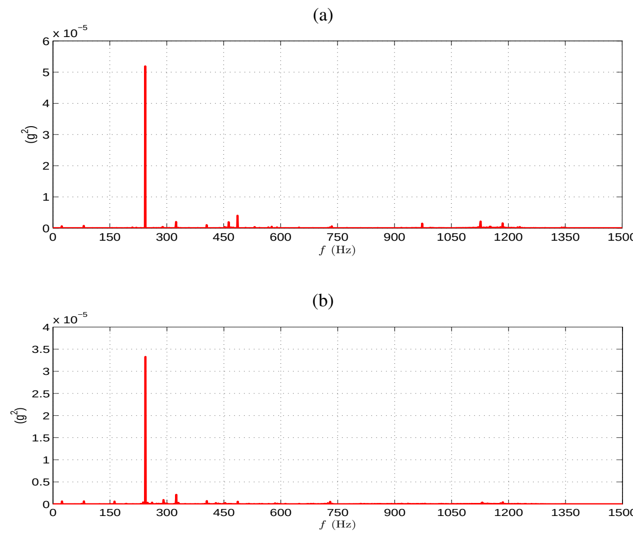

Fig. 4. Power spectral density of the AHB: baseline (00321) in (a), and misaligned (20321) in (b)

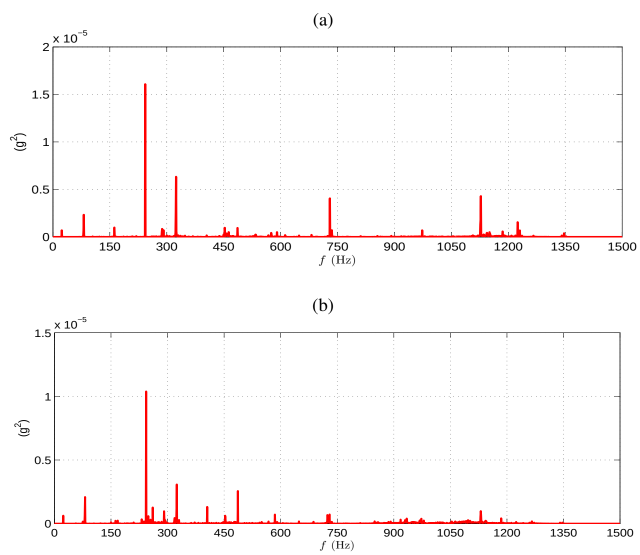

Fig. 5. Power spectral density of the AHB: unbalanced (10321) in (a), and misaligned-unbalanced (30321) in (b)

peaks (SP1, SP2, and SP3) of the faulted drive-shafts (first three harmonics of the shaft rotating speed (81Hz, 162Hz and 243Hz)). As shown in Table II, values of the SP2 for all faulted cases exceed the 6 dB threshold compared to the baseline and therefore it provides a good indicator for all of the three faulted cases. In fact, SP2 is currently employed in the HUMS system to detect unbalanced and/or misaligned shafts in a tail rotor drive-train of a rotorcraft [30]. However, this Condition Indicator (CI) has limited diagnostic capabilities in specifying whether the fault is unbalance, misalignment or a combination of both faults. The maintainers are told to check for more than one source that might cause that CI to exceed its limit.

The vibration data is then investigated using the proposed $QNLPI(f)$ discussed in section II. Figure 6-(a) shows $QNLPI(f)$ spectrum for the baseline case for which nonlinearly-generated frequencies located at 1^{st} and 7^{th} har-

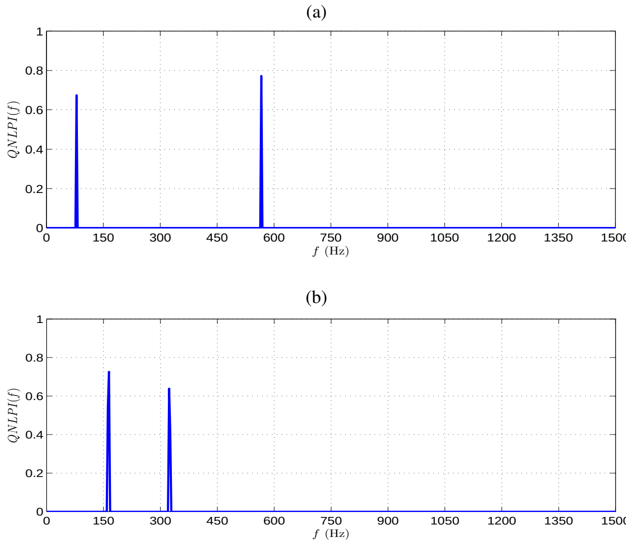

Fig. 6. $QNLPI$ of the AHB: baseline (00321) in (a), and misaligned (20321) in (b)

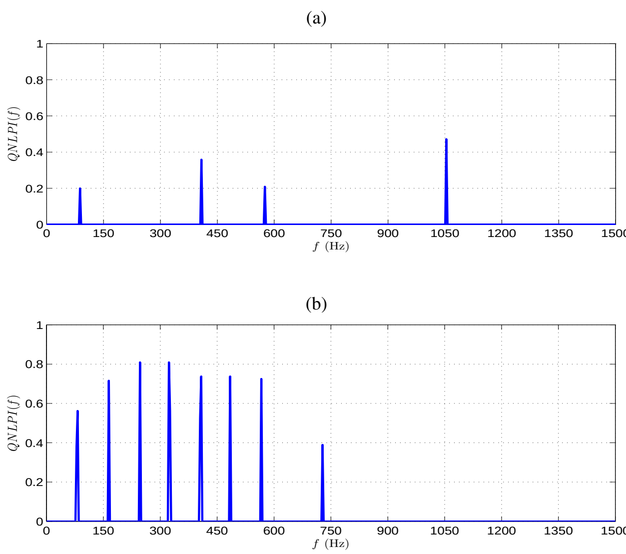

Fig. 7. QNLPI of the AHB: unbalanced (10321) in (a), and misaligned-unbalanced (30321) in (b)

monics of the drive-shaft with values 0.68 and 0.77, respectively. These values can be result of interaction between the dominating 3^{rd} harmonic with the 4^{th} to produce 68% and 77% of the power at 1^{st} and 7^{th} harmonics, respectively. The remaining fraction of the power may be independently excited or coming from other forms of nonlinearities. Due to different experimental settings, different interaction pattern exists in the case of misalignment as shown in Figure 6-(b). In this case, quadratic nonlinear interaction between the 3^{rd} and the 1^{st} harmonics is dominating. As a result of this interaction, 2^{nd} and 4^{th} harmonics are generated with power fraction of 0.72 and 0.64, respectively. The results in Figure 6 give us more details about the content of the power spectrum of the signal. Some frequencies in common between the baseline and misaligned cases have different origins. For example, the 1^{st} and the 4^{th} harmonics exchange there places as source/result of the interaction process with the 3^{rd} due to different physical setting of the rotating shaft.

Comparing the $QNLPI(f)$ of the unbalance case shown in Figure 7-(a) with the baseline case in Figure 6-(a), we can see a slightly more interaction introduced in the case of the unbalance. The 4^{th} harmonic interacts with both 3^{rd} and 9^{th} producing a series of odd harmonics at 1^{st}, 5^{th}, 7^{th}, and 13^{th}. The increasing production of odd harmonics through the nonlinear interaction is likely a sign of unbalance. On the other hand, as discussed above, the production of even harmonics is likely a sign of misalignment. Thus, when a combination of unbalance and misalignment is introduced to the drive-shafts, one can expect that nonlinearity of the system will increase so that a variety of odd/even harmonics of the drive shaft rotating frequency is produced as shown in Figure 7-(b).

From the discussion above, we can see that beside conventional power spectral density analysis, using $QNLPI(f)$ spectrum helps to gain more details about nonlinear harmonic interaction/generation patterns, which can be used to distinguish between different fault settings of the tail rotor drive-shafts.

C. *Studying Progress of Gearbox fault using* $QNLPI(f)$

In this subsection, we use vibration data collected in the experimental TRDT test stand to study tail-rotor gearbox failure (denoted TRGB in Figure 3) due to lubrication starvation [31]. This experiment was originally designed to demonstrate whether or not a gearbox with a leaking output seal could be used in the filed until the aircraft reached a phase inspection, which currently occurs every 250 hours. The output seals were seeded to represent a worst-case scenario leak for gearboxes. For all the tested articles, it was observed that a persistent grease leak through the output seal resulted in a loss of lubricant in the main gear compartment. Consequently, this condition ultimately resulted in lubricant starvation on the gear meshing region and catastrophic gear teeth failures, as shown in Figure 8. One interesting finding of this experiment was that gearbox can survive more than 480 hours after fault seeding for all tested articles. The secondary objective of the experiment was to identify vibration signatures which might indicate the impending failure. Here, we use vibration data collected from this experiment to illustrate the usefulness of the proposed index in keeping track of the progress of fault in the gearbox.

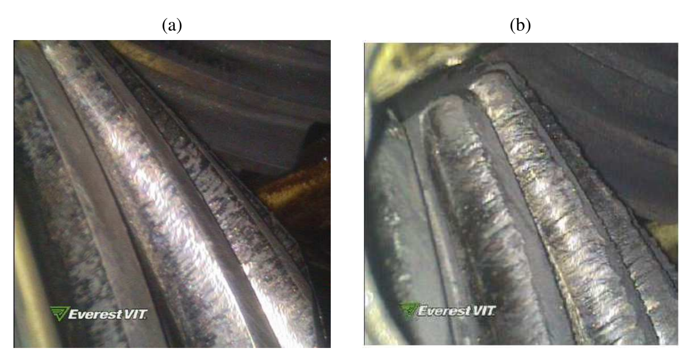

Fig. 8. Borescope picture showing input gear teeth: (a) earlier stage of testing, and (b) after failure [31]

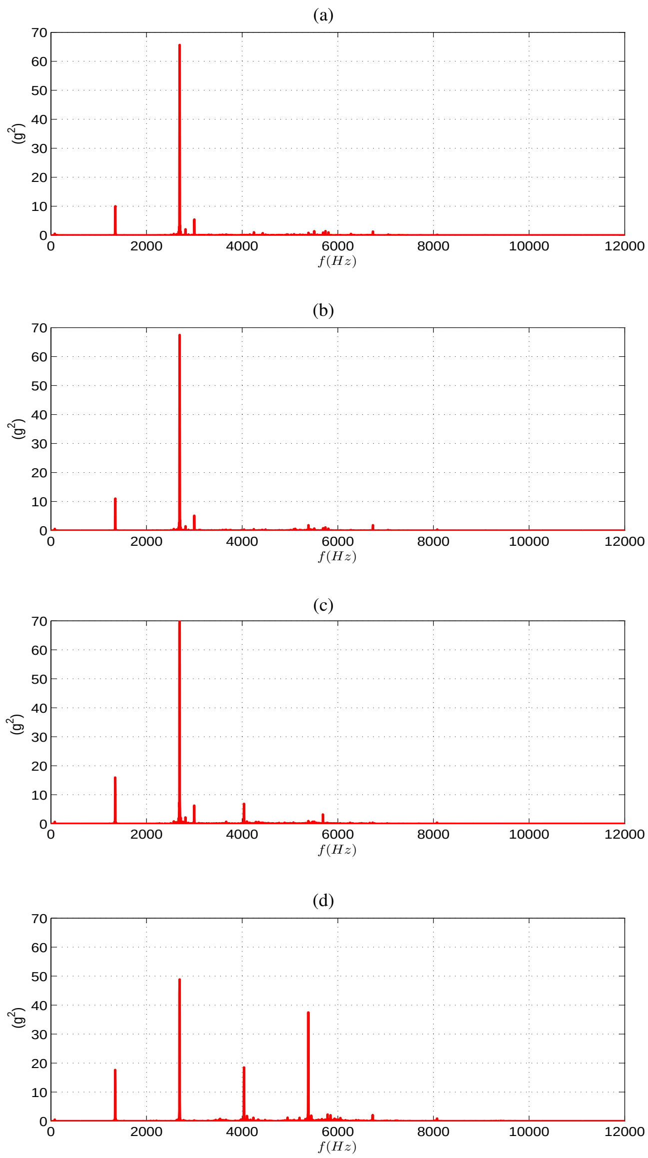

Fig. 9. Progress of power spectral density (PSD) change during gear teeth failure: (a) 3 days before failure, (b) 2 days before failure, (c) 1 days before failure, and (d) same day of failure

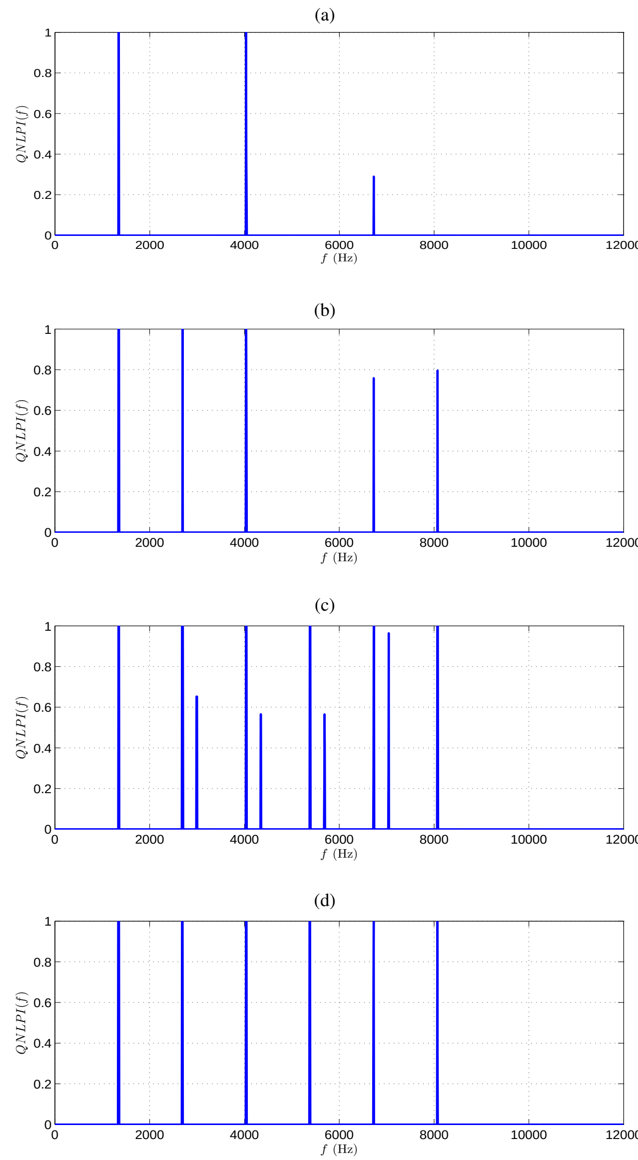

Fig. 10. Progress of nonlinear harmonic generation due to gear teeth failure: (a) 3 days before failure, (b) 2 days before failure, (c) 1 days before failure, and (d) same day of failure

Figure 9 shows how the average power spectral density (PSD) of the gearbox vibration changes during the last four days before failure. Inspection of the PSD plots indicates that it was not until the day of failure that vibration power at the third and fourth harmonics of the gear mesh frequency (1334Hz) increased suddenly to warning values, as shown in Figure 9-(d). During the last three days preceding the failure, shown in Figure 9-(a) $\sim$ (c), PSD stayed almost the same with slightly monotonic increase of vibration power at the both first and second harmonics of the gear mesh frequency.

Progress of failure developed in the gearbox is studied using the proposed $QNLPI(f)$, as shown in Figure 10-(a) $\sim$ (d), for the same vibration data set which studied previously in Figure 9. Figure 10-(a) shows the $QNLPI(f)$ of gearbox vibration three days before gearbox failure which has the least quadratic-nonlinearly produced frequencies with only first, third, and fifth mesh harmonics having $QNLPI$ equal to 1, 1, and 0.33, respectively. Two days before failure, vibration nonlinearity increased causing the values of $QNLPI$ at the pre-exist harmonics to increase, and more nonlinearity to show up at the second and sixth harmonics, as seen in Figure 10-(b). The highest nonlinearity in the vibration signal is exist one day before failure as shown in Figure 10-(c). On that day, beside the high nonlinearity at all the first six harmonics of the TRGB, gear mesh frequency of the intermediate gearbox (IGB), 3000 Hz, shows up interacting with several TRGB harmonics. This IGB frequency disappeared in the day of failure from the $QNLPI(f)$ spectrum, but all gear mesh harmonics of the faulted TRGB stayed at high nonlinear power values, as shown in Figure 10-(d). This consistent increase in the nonlinear production/coupling of gear meshing harmonics, regardless of there power spectral values, can be used as precocious indication of gear-teeth failure.

In order to describe the progress of fault in the gearbox using single-valued metric, percentage of quadratic nonlinear power ($PQNLP$) in equation (8) is employed. Figure 11 compares the progress of the $PQNLP$ to other condition indicators during the last four days of experiment. The $1GMF$ and $2GMF$ are the vibration spectral peaks at the first and the second harmonics of the gear mesh frequency. The root-mean-square (RMS) and the energy-ratio (ER) condition indicators are calculated as reported in [9] to describe heavy gear wear.

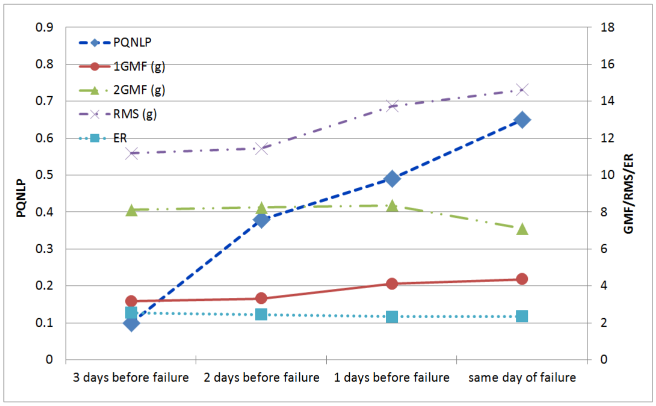

Fig. 11. Trend of vibration $PQNLP$ compared to different condition indicators for the faulted TRGB during the last four days before failure

As shown in Figure 11, the value of $PQNLP$ starts showing considerable increase one day before other condition indicators. It is consistently climbing up until the gearbox failure due to wear in the input gear teeth which physically can be interpreted as increased vibration power due to highly-nonlinear rotating medium. Thus, this trend can be used as precocious indication of failure. The advantage of using $PQNLP$ as condition indicator over conventional power spectrum indicators is the inherent characteristics of HOS-based metrics as amplification invariance and high immunity to additive Gaussian noise, which reduce the dependency on the characteristics of the sensor used to collect the vibration data.

IV. Conclusion

The quadratic-nonlinearity power-index ($QNLPI(f)$) has been proposed which provides a summary of the nonlinearity information contained in the the 3D bicoherence into 2D spectrum presenting an easier way to studying third-order statistic of signals. The proposed index inherits useful characteristics of the bicoherence such as high immunity to additive gaussian noise, and amplification invariance; two properties of interest in practical applications to relax the pardon on sensors used in collecting time-varying waveforms.

The proposed index has been used to study real-world vibration data collected from tail-rotor drive train of an AH-64 helicopter. Two case studies have been conducted. In the first case, $QNLPI(f)$ has shown better diagnostic capabilities in differentiating between different drive-shaft faults by showing how different physical settings affect the nonlinear generation of harmonics. In the second case, $QNLPI(f)$ has shown better capability in detecting gearbox failure. For easier monitoring of the fault-progress in the gearbox, percentage of total quadratic nonlinear power ($PQNLP$) has been calculated based on the proposed $QNLPI(f)$ and has shown consistent increase during the gear fault aging. This single-valued metric can be used in prognostic models to estimate the remanding useful life of mechanical components.

It is worthwhile to mention here that although the proposed metrics provide more accurate tools to diagnose mechanical faults compared to the conventional power spectral analysis, this comes at the cost of computational resources and time. The computational complexity is $O(N^2)$ where N is the number of points in one signal realization. For example, for N= 4096, it takes 34.517 sec to compute the $QNLPI(f)$, while it takes 0.251 sec to compute the power spectral density using the same platform.

Future research in this area includes studying the effect of loading by the trail-rotor blades on the proposed metrics, and extending the application of the proposed metrics to study more faults and failure modes in aircrafts and similar rotating systems such wind turbines. The unique nonlinearity signature of each fault can be used to design more accurate and reliable diagnostic algorithms for the condition based maintenance (CBM) practice.

Appendix
Boundary limits of $QNLPI(f)$

Assume that the signal at frequency m, $X(m)$, is constructed from finite number of quadratic coupling pairs plus non-quadratic coupling part as shown in equation (10).

$$X(m) = \sum_{\forall\, l+k=m} A_{l,k}\, X(l)X(k) + X^{'}(m) \tag{10}$$

where $A_{l,k}$ is the coupling coefficient between two frequencies l and k to produce sum frequency m. $X^{'}(m)$ represents any non-quadratic coupling power in the signal, either independent excitation or from other higher order interactions. Assuming that $x(t)$ is a zero-mean wide-sense stationary random signal, the mean square power at frequency m, $P_x(m)$, can be proven to be as follows [27];

$$P_x(m) = \sum_{(\forall\, l+k=m)} |A_{l,k}|^2\, E\{|X(l)X(k)|^2\} + E\{|X^{'}(m)|^2\} \tag{11}$$

First part of equation (11) represents the total power at frequency m due to all quadratic coupling pairs, while the second part is due to any non-quadratic-coupling power at this frequency. Substituting from equation (2) in equation (4),

$$QNLPI(m) = \int_{0}^{f_s/4} \frac{|E\{X(\frac{m}{2}+f_1)X(\frac{m}{2}-f_1)X^{*}(m)\}}{P_x(m)\cdot E\{|X(\frac{m}{2}+f_1)X(\frac{m}{2}-f_1)|^2\}}\, df_1 \tag{12}$$

Then, from equation (10) in equation (12) recalling properties of expected value operator, we get the following equation:

$$QNLPI(m) = \frac{1}{P_x(m)} \int_{0}^{f_s/4} \left(\frac{|A+B|^2}{C}\right) df_1 \tag{13}$$

where,

$$A = \sum_{\forall\, l+k=m} A_{l,k}\, E\left\{X(\frac{m}{2}+f_1)X(\frac{m}{2}-f_1)X^*(l)X^*(k)\right\}$$

$$B = E\left\{X(\frac{m}{2}+f_1)X(\frac{m}{2}-f_1)X^{'*}(m)\right\}$$

$$C = E\left\{|X(\frac{m}{2}+f_1)X(\frac{m}{2}-f_1)|^2\right\}$$

The value of the expected value operators in the numerator of equation (13) will be zero except when variable f_1 equals to $f_1 = \frac{m}{2} - l = \frac{m}{2} + k$. Therefore, integration in equation (13) is reduced to summation as follows:

$$QNLPI(m) = \frac{\sum\limits_{\forall l+k=m} |A_{l,k}|^2 E\{|X(l)X(k)|^2\}}{P(m)} \tag{14}$$

Note that numerator of equation (14) represents the total power at frequency m due to all quadratic coupling pairs and it is fraction of $P_x(m)$ as shown before in equation (11). Hence, the proposed index, $QNLPI(m)$, measures the fraction of the mean square power at frequency m due to quadratic coupling between all combination of frequencies that possibly result in m. Also, from (14), $0 \le QNLPI(m) \le 1$, and will equal one if, and only if, $X^{'}(m) = 0$.

Acknowledgment

This research is funded by the South Carolina Army National Guard and United States Army Aviation and Missile Command via the Conditioned-Based Maintenance (CBM) Research Center at the University of South Carolina-Columbia. Also, this research is partially supported by the Egyptian government under the Government Mission Program for Mr. Mohammed Hassan. This work was supported in part by the National Science Foundation under Grant 0747681. Also, this work was supported in part by the Yonsei University Research Fund of 2012.

References

[1] A. K. S. Jardine, D. Lin, and D. Banjevic, "A review on machinery diagnostics and prognostics implementing condition-based maintenance," *Mechanical Systems and Signal Processing*, vol. 20, no. 7, pp. 1483-1510, Oct. 2006.

[2] A. Heng, S. Zhang, A. C. Tan, J. Mathew, "Rotating machinery prognostics: State of the art, challenges and opportunities," *Mechanical Systems and Signal Processing*, vol. 23, no. 3, pp. 724-739, Apr. 2009.

[3] H. M. Hashemian, W. C. Bean, "State-of-the-art predictive maintenance techniques," *IEEE Transactions on Instrumentation and Measurement*, vol. 60, no. 10, pp. 3480-3492, Oct. 2011.

[4] R. Li, D. He, "Rotational machine health monitoring and fault detection using EMD-based acoustic emission feature quantification," *IEEE Transactions on Instrumentation and Measurement*, vol. 61, no. 4, pp. 990-1001, Apr. 2012.

[5] J. Yu, "Health condition monitoring of machines based on hidden markov model and contribution analysis," *IEEE Transactions on Instrumentation and Measurement*, vol. 61, no. 8, pp. 2200-2211, Aug. 2012.

[6] A. Bayoumi, W. Ranson, L. Eisner, and L.E. Grant, "Cost and effectiveness analysis of the AH-64 and UH-60 on-board vibrations monitoring system," *IEEE Aerospace Conference,* pp. 3921-3940, Mar. 2005.

[7] D. Coats, Cho Kwangik, Yong-June Shin, N. Goodman, V. Blechertas, and A. Bayoumi, "Advanced time-frequency mutual information measures for condition-based maintenance of helicopter drivetrains," *IEEE Transactions on Instrumentation and Measurement*, vol. 60, no. 8, pp. 2984-2994, Aug. 2011.

[8] G. Betta, C. Liguori, A. Paolillo, and A. Pietrosanto, "A DSP-based FFT-analyzer for the fault diagnosis of rotating machine based on vibration analysis," *IEEE Transactions on Instrumentation and Measurement*, vol. 51, no. 6, pp. 1316-1322, Dec. 2002.

[9] P. D. Samuel, and D. J. Pines, "A review of vibration-based techniques for helicopter transmission diagnostics," *Journal of Sound and Vibration*, vol. 282, no. 1-2, pp. 475-508, Apr. 2005.

[10] A. S. Sait, and Y. I. Sharaf-Eldeen, "A review of gearbox condition monitoring based on vibration analysis techniques diagnostics and prognostics," in *Rotating Machinery, Structural Health Monitoring, Shock and Vibration*, Vol. 8, T. Proulx, Ed. New York: Springer, 2011, pp. 307-324.

[11] W. Bartelmus, R. Zimroz, "Vibration condition monitoring of planetary gearbox under varying external load," *Mechanical Systems and Signal Processing*, vol. 23, no. 1, pp. 246-257, Jan. 2009.

[12] R. B. Randall, J. Antoni, "Rolling element bearing diagnostics-A tutorial," *Mechanical Systems and Signal Processing*, vol. 25, no. 2, pp. 485-520, Feb. 2011.

[13] J. Dybala, "Vibrodiagnostics of gearboxes using NBV-based classifier: A pattern recognition approach," *Mechanical Systems and Signal Processing*, vol. 38, no. 1, pp. 522, July 2013.

[14] T. W. S. Chow, and Gou Fei, "Three phase induction machines asymmetrical faults identification using bispectrum," *IEEE Transactions on Energy Conversioin*, vol. 10, no. 4, pp. 688-693, Dec. 1995.

[15] N. Arthur, and J. Penman, "Induction machine condition monitoring with higher order spectra," *IEEE Transactions on Industrial Electronics*, vol. 47, no. 5, pp. 1031-1041, Oct. 2000.

[16] T. W. S. Chow, and H.-Z. Tan, "HOS-based nonparametric and parametric methodologies for machine fault detection," *IEEE Transactions on Industrial Electronics*, vol. 47, no. 5, pp. 1051-1059, Oct. 2000.

[17] B. Jang, C. Shin, E. J. Powers, and W. M. Grady, "Machine fault detection using bicoherence spectra," *Proceeding of the IEEE Instrumentation and Measurement Technology Conference*, vol. 3, no. 1, pp. 1661-1666, May 2004.

[18] T. Kim, W. Cho, E. J. Powers, W. M. Grady, and A. Arapostathis, "ASD system condition monitoring using cross bicoherence," *Proceeding of the IEEE electricship technologies symposium*, pp. 378-383, May 2007.

[19] M. A. Hassan, D. Coats, K. Gouda, Yong-June Shin, and A. Bayoumi, "Analysis of nonlinear vibration-interaction using higher order spectra to diagnose aerospace system faults," *Proceeding of the IEEE Aerospace Conference*, pp. 1-8, March 2012.

[20] J. K. Sinha, K. Elbhbah, "A future possibility of vibration based condition monitoring of rotating machines," *Mechanical Systems and Signal Processing*, vol. 36, no. 1-2, pp. 231240, Jan. 2013.

[21] T-T. Ng, S-F. Chang, and Q. Sun, "Blind detection of photomontage using higher order statistics," *Proceeding of the IEEE International Symposium on Circuits and Systems (ISCAS)*, vol. 5, pp. 688-691, May 2004.

[22] K. C. Chua, V. Chandran, U. R. Acharya, and C. M. Lim, "Cardiac state diagnosis using higher order spectra of heart rate variability," *Journal of Medical Engineering & Technology*, vol. 32, no. 2, pp. 145155, March/April 2008.

[23] V. Chandran, and S. Elgar, "Pattern recognition using invariants defined from higher order spectra- One dimensional inputs," *IEEE Transactions on Signal Processing*, vol. 41, no. 1, pp. 205-212, Jan. 1993.

[24] V. Chandran, S. Elgar, and A. Nguyen, "Detection of mines in acoustic images using higher order spectral features," *IEEE Journal of Oceanic Engineering*, vol. 27, pp. 610- 618, Jul 2002.

[25] M. A. Hassan, D. Coats, Yong-June Shin, and A. Bayoumi, "Quadratic-nonlinearity power-index spectrum and its application in condition based maintenance (CBM) of helicopter drive trains," *Proceeding of the IEEE International Instrumentation and Measurement Technology Conference (I2MTC)*, pp. 1456-1460, May 2012.

[26] Boualem Boashash, Edward J. Powers, Abdelhak M. Zoubir, "*Higher-Order Statistical Signal Processing,*" Wiley, 1996.

[27] Y. C. Kim, and E. J. Powers, "Digital bispectral analysis and its application to nonlinear wave interactions," *IEEE Transactions on Plasma Science*, vol. 7, no. 2, pp. 120-131, July 1979.

[28] John G. Proakis, and Dimitris G. Manolakis, "Power spectrum estimation," in *Digital Signal Proccessing: Principles, Algorithms, and Applications*, 4th ed. New Jersey: Prentice Hall, 2007, pp. 960-1040.

[29] R. B. Randall, "Fault detection," in *Vibration-Based Condition Monitoring: Industrial, Aerospace and Automotive Applications,* Wiley, 2011.

[30] P. Grabill, J. Seale, D. Wroblewski, and T. Brotherton, "iTEDS: the intelligent turbine engine diagnostic system," *Proceedings of 48 International Instrumentaion Symposium*, pp. 345-353, May 2002.

[31] N. Goodman, A. Bayoumi, V. Blechertas, R. Shah, and Yong-June Shin, "CBM component testing at the university of south carolina: AH-64 tail rotor gearbox studies," *Presented at the American Helicopter Society Technical Specialists Meeting on Condition Based Maintenance*, Huntsville, AL, pp. 1-8, Feb. 2009.

Mohammed A. Hassan M.Sc., received the B.S. degree with honors in Electrical Engineering from Cairo University, Fayoum Campus, Fayoum, Egypt, and the M.Sc. degree in Electronics and Communication Engineering from Cairo University, Cairo, Egypt, in 2001 and 2004, respectively. He is currently pursuing his PhD degree in the Electrical Engineering Department at the University of South Carolina. His current research interests include advanced digital signal processing techniques: time-frequency analysis and higher order statistical signal processing, and their applications in condition based maintenance.

Abdel-Moez E. Bayoumi Ph.D., Director of the USC Biomedical Engineering Program and Professor of Mechanical Engineering at the University of South Carolina- Columbia. He chaired the Department of Mechanical Engineering from 1998 through 2006. Before joining USC, he was a Professor and Director of the Manufacturing Program at North Carolina State University-Raleigh, North Carolina (1996-1998); Assistant, Associate, Professor, and Distinguished Boeing Manufacturing Professor at Washington State University (1983-1996); a Project Manager at Hewlett-Packard Company-Corvallis, Oregon (1993-1995 - on professional leave from WSU); and a visiting scholar for a year at the American University in Cairo (AUC) - Egypt (1991-1992 - a sabbatical leave from WSU). During his tenure at the University of South Carolina, North Carolina State University, Washington State University, the American University in Cairo, and Hewlett-Packard Company, Dr. Bayoumi has been actively involved in developing strong research and educational programs. His current areas of interest can be grouped into three categories, (1) Study of Condition-Based Maintenance (CBM) of military aircraft in which diagnosis, prognosis and health monitoring systems are effectively utilized using informatics and sensing technologies, (2) Micro-Electro Mechanical Systems (MEMS) and Mechatronics in which a MEMS device is designed, fabricated and used to sense and control mechanical or biological systems, and (3) Design and applications of efficient energy resources and system.

Yong-June Shin Ph.D., received his B.S. degree from the Department of Electrical Engineering, Yonsei University, Seoul, Korea, in 1996 with early completion honors and the M.S. degree from The University of Michigan, Ann Arbor, in 1997. He received the Ph.D. degree from the Department of Electrical and Computer Engineering, The University of Texas at Austin, in 2004. Upon his graduation, he joined the Department of Electrical Engineering, The University of South Carolina as an Assistant Professor. He was promoted to Associate Professor with tenure in 2011. He joined School of Electrical and Electronic Engineering, at Yonsei University, Seoul, Korea since September 2012. He is a recipient of the United States National Science Foundation CAREER award in year 2008, and General Electric Korean-American Education Commission Scholarship. Dr. Shin's current research interests are characterized by the application of novel digital signal processing techniques to a wide variety of important transient and nonlinear problems in smart electric power grid.